Chapter Eight

# Quantum Monte Carlo Applied to the Spin-$\frac{1}{2}$ Easy-Plane Ferromagnet CHAB

## 8.1 Vertex Energies for a General Spin-$\frac{1}{2}$ Model

In the notation of Chapter 7, the following general spin-$\frac{1}{2}$ Hamiltonian is considered here:

$$\hat{H}^{\circ}_{n,n+1} = -J_z \hat{S}^z_n \hat{S}^z_{n+1} - \tfrac{1}{2} g\mu_B B_z (\hat{S}^z_n + \hat{S}^z_{n+1}) \tag{8-1a}$$

$$\hat{V}_{n,n+1} = -J_x \hat{S}^x_n \hat{S}^x_{n+1} - J_y \hat{S}^y_n \hat{S}^y_{n+1} - \tfrac{1}{2} g\mu_B B_x (\hat{S}^x_n + \hat{S}^x_{n+1}) \quad . \tag{8-1b}$$

$\hat{S}^x_n$, $\hat{S}^y_n$ and $\hat{S}^z_n$ are spin-$\frac{1}{2}$ operators, related to the usual Pauli spin matrices $\vec{\sigma}_n$ by

$$\hat{S}^{\alpha}_n = \tfrac{1}{2} \hat{\sigma}^{\alpha}_n \quad , \quad \alpha = x, y, z, \quad n = 1, 2, \ldots N. \tag{8-2}$$

$J_x$, $J_y$ and $J_z$ are arbitrary exchange constants, and $B_x$ and $B_z$ are applied fields. For the easy-plane ferromagnet, all the J's are positive, and two of them are equal; for example, $J_x = J_y$, with $J_z < J_x$. Note that for a quantum spin-$\frac{1}{2}$ model the anisotropy must be in the exchange terms since $(\hat{\sigma}^z_n)^2 = 1$. Only higher spin-S models can have single ion anisotropies.

First the vertex weights (the matrix elements) in equation (7-12) will be calculated, using eigenstates of the $\hat{S}^z_n$ operators. The effect of $\hat{H}^{\circ}_{n,n+1}$ is trivial, such that the vertex weight $w_{n,r}$ is

$$w_{n,r} = e^{-\beta E_{n,r}} = e^{-\beta E^{\circ}_{n,r}} \langle S_{n,r} S_{n+1,r} | e^{-\frac{\beta}{m} \hat{V}_{n,n+1}} | S_{n,r+1} S_{n+1,r+1} \rangle \tag{8-3a}$$

where

$$E^{o}_{n,r} = -\frac{1}{2m}[J_z(S_{n,r}S_{n+1,r} + S_{n,r+1}S_{n+1,r+1}) + \frac{1}{2}g\mu_B B_z(S_{n,r} + S_{n+1,r} + S_{n,r+1} + S_{n+1,r+1})] \quad . \tag{8-3b}$$

Matrix elements of $\exp(-\frac{\beta}{m}\hat{V}_{n,n+1})$ are more involved. Making the following definitions of rescaled parameters,

$$K_{x,y,z} = \frac{\beta J_{x,y,z}}{4m} \quad , \quad b_{x,z} = \frac{\beta}{4m} g\mu_B B_{x,z} \quad , \tag{8-4a}$$

$$\alpha = \frac{g\mu_B B_x}{J_y} = \frac{b_x}{K_y} \quad , \tag{8-4b}$$

then we want the exponential of the operator $\hat{M}$,

$$\hat{M} \equiv -\frac{\beta}{m}\hat{V}_{n,n+1} = K_x\hat{a} + K_y(\hat{b} + \alpha\hat{c}) \quad , \tag{8-5a}$$

where

$$\hat{a} \equiv \hat{\sigma}^x_n\hat{\sigma}^x_{n+1} \quad , \quad \hat{b} \equiv \hat{\sigma}^y_n\hat{\sigma}^y_{n+1} \quad , \quad \hat{c} \equiv \hat{\sigma}^x_n + \hat{\sigma}^x_{n+1} \quad . \tag{8-5b}$$

The exponential is simplified first by noticing that $\hat{a}$ and $\hat{b}$ commute so that

$$e^{\hat{M}} = e^{K_x\hat{a}}\, e^{K_y(\hat{b}+\alpha\hat{c})} = (\cosh K_x + \hat{a}\sinh K_x)e^{K_y(\hat{b}+\alpha\hat{c})} \quad . \tag{8-6}$$

To expand the remaining exponential,

$$e^{K_y(\hat{b}+\alpha\hat{c})} = \sum_{p=0}^{\infty} \frac{K_y^{2p}}{(2p)!}(\hat{b}+\alpha\hat{c})^{2p} + \sum_{p=0}^{\infty} \frac{K_y^{2p+1}}{(2p+1)!}(\hat{b}+\alpha\hat{c})^{2p+1} \quad , \tag{8-7}$$

consider the even powers first. We want a general formula for $(\hat{b} + \alpha\hat{c})^{2p}$. Using the following easily verified identities,

$$\hat{a}^2 = \hat{b}^2 = 1 \tag{8-8a}$$

$$\{\hat{b}, \hat{c}\} = 0 \tag{8-8b}$$

$$\hat{c}^2 = 2(1+\hat{a}) \quad , \tag{8-8c}$$

then one obtains

$$(\hat{b} + \alpha\hat{c})^{2p} = 1 + \frac{1}{2}[(1+4\alpha^2)^p - 1](1+\hat{a}) \quad . \tag{8-9}$$

Similarly, the odd powers can be written

$$(\hat{b} + \alpha\hat{c})^{2p+1} = \frac{1}{2}[(\hat{b}+\hat{d}) + (1+4\alpha^2)^p(\hat{b}-\hat{d} + 2\alpha\hat{c})] \tag{8-10a}$$

where

$$\hat{d} \equiv \hat{\sigma}^z_n\hat{\sigma}^z_{n+1} \quad . \tag{8-10b}$$

Then summing the exponential series leads to the identify

$$2e^{K_y(\hat{b}+\alpha\hat{c})} = (1-\hat{a})\cosh K_y + (1+\hat{a})\cosh K_y(1+4\alpha^2)^{1/2}$$

$$+ (\hat{b}+\hat{d}) \sinh K_y + (\hat{b}-\hat{d} + 2\alpha\hat{c})(1 + 4\alpha^2)^{-1/2}\sinh K_y(1 + 4\alpha^2)^{1/2} \quad . \tag{8-11}$$

Substituting this into (8-6) finally gives an operator result from which matrix elements are directly obtained

$$2e^{\hat{M}} = [e^{K_x}(\cosh K_b - \gamma \sinh K_b) + e^{-K_-}] \frac{1}{2}(1 + \hat{\sigma}^z_n\hat{\sigma}^z_{n+1})$$

$$+ [e^{K_x}(\cosh K_b + \gamma \sinh K_b) + e^{-K_+}] \frac{1}{2}(1 - \hat{\sigma}^z_n\hat{\sigma}^z_{n+1})$$

$$+ [e^{K_x}(\cosh K_b + \gamma \sinh K_b) - e^{-K_+}](\hat{S}^+_n\hat{S}^-_{n+1} + \hat{S}^-_n\hat{S}^+_{n+1})$$

$$+ [e^{K_x}(\cosh K_b - \gamma \sinh K_b) - e^{-K_-}] (\hat{S}_n^+\hat{S}_{n+1}^+ + \hat{S}_n^-\hat{S}_{n-1}^-)$$

$$+ (2\alpha\gamma e^{K_x} \sinh K_b)(\hat{S}_n^+ + \hat{S}_n^- + \hat{S}_{n+1}^+ + \hat{S}_{n+1}^-) \quad , \tag{8-12}$$

where

$$K_\pm = K_x \pm K_y \tag{8-13a}$$

$$\gamma = (1 + 4\alpha^2)^{-1/2} \tag{8-13b}$$

$$K_b = K_y/\gamma \quad . \tag{8-13c}$$

For this spin-$\frac{1}{2}$ model, since there are 4 spins in a vertex, and 2 states per spin, there are 16 possible vertices (in the general spin-S case, there will be $(2S + 1)^4$ possible vertices). All are nonzero if $B_x \neq 0$ (16 vertex model), while 8 are nonzero if $B_x = 0$ and $J_x \neq J_y$ (8 vertex model). Only 6 are nonzero if $B_x = 0$ and $J_x = J_y$; this is then the isotropic 6 vertex model studied by Cullen and Landau (1983). It is seen that the presence of symmetries tends to reduce the number of allowed vertices. If a given vertex weight is zero, then the vertex has infinite energy and is prohibited. If a given vertex weight is negative, then the energy is complex, and the standard Monte Carlo algorithm may need modification (or not be applicable at all), unless these vertices always occur in pairs, such that the net weight of the state for the whole system is positive. For present purposes we deal only with models where all the vertices have non-negative weights.

## 8.2 The Effective Hamiltonian for the 2-D Lattice

It is possible to write the vertex weights for all 16 possible

vertices in terms of a single interaction, or effective Hamiltonian on the 2-D lattice. We will consider first the case where $B_z = 0$ and $B_x \neq 0$.

Using u to indicate spin up $(+\frac{1}{2})$ and d to indicate spin down $(-\frac{1}{2})$, we can form the following list of vertex weights (from equations 8-3 and 8-12) in Cullen and Landau's notation

$$\begin{matrix} u\ u \\ u\ u \end{matrix} \quad w_1 = \tfrac{1}{2}[e^{K_x}(\cosh K_b - \gamma \sinh K_b) + e^{-K_-}]e^{K_z+2b_z}$$

$$\begin{matrix} d\ d \\ d\ d \end{matrix} \quad w_2 = \tfrac{1}{2}[e^{K_x}(\cosh K_b - \gamma \sinh K_b) + e^{-K_-}]e^{K_z-2b_z}$$

$$\begin{matrix} u\ d \\ u\ d \end{matrix} \quad w_3 = \tfrac{1}{2}[e^{K_x}(\cosh K_b + \gamma \sinh K_b) + e^{-K_+}]e^{-K_z}$$

$$\begin{matrix} d\ u \\ d\ u \end{matrix} \quad w_4 = w_3$$

$$\begin{matrix} d\ u \\ u\ d \end{matrix} \quad w_5 = \tfrac{1}{2}[e^{K_x}(\cosh K_b + \gamma \sinh K_b) - e^{-K_-}]e^{-K_z}$$

$$\begin{matrix} u\ d \\ d\ u \end{matrix} \quad w_6 = w_5$$

$$\begin{matrix} d\ d \\ u\ u \end{matrix} \quad w_7 = \tfrac{1}{2}[e^{K_x}(\cosh K_b - \gamma \sinh K_b) - e^{-K_x}]e^{K_z}$$

$$\begin{matrix} u\ u \\ d\ d \end{matrix} \quad w_8 = w_7$$

$$\begin{matrix} d\ u \\ u\ u \end{matrix}, \begin{matrix} u\ u \\ d\ u \end{matrix}, \begin{matrix} u\ u \\ u\ d \end{matrix}, \begin{matrix} u\ d \\ u\ u \end{matrix} \quad w_{9,10,11,12} = \alpha\gamma e^{K_x+b_z} \sinh K_b$$

$$\begin{matrix} u\ d \\ d\ d \end{matrix}, \begin{matrix} d\ d \\ u\ d \end{matrix}, \begin{matrix} d\ d \\ d\ u \end{matrix}, \begin{matrix} d\ u \\ d\ d \end{matrix} \quad w_{13,14,15,16} = \alpha\gamma e^{K_x-b_z} \sinh K_b \quad . \qquad (8\text{-}14)$$

In these diagrams the vertical direction is the Trotter direction and the horizontal direction is the spatial direction.

In the following, a simple notation for the spins in a vertex will be convenient. We will use

$$\begin{matrix} S_{n,r+1} & S_{n+1,r+1} \\ S_{n,r} & S_{n+1,r} \end{matrix} = \begin{matrix} S_4 & S_3 \\ S_1 & S_2 \end{matrix} \tag{8-15}$$

We want to form "classical spin operators" that is, combinations of $S_1$, $S_2$, $S_3$ and $S_4$ which are zero for all but one of the vertices. Actually we only need classical spin operators which distinguish between vertices with different weights; the same operator will apply to vertices 9 through 12, for instance. Simplest to consider are products such as $S_1S_2$ and $S_1S_2S_3S_4$. Consider the following classical spin products

$$\begin{aligned} x &\equiv 2(S_1S_2 + S_3S_4) \quad , \quad \text{horizontal coupling,} \\ y &\equiv 2(S_1S_4 + S_2S_3) \quad , \quad \text{vertical coupling,} \\ z &\equiv 2(S_1S_3 + S_2S_4) \quad , \quad \text{diagonal coupling,} \\ q &\equiv 16\, S_1S_2S_3S_4 \quad , \quad 4 \text{ spin coupling.} \end{aligned} \tag{8-16}$$

For the case where $B_z = 0$, which we take for the moment, there are only five distinct vertex weights: $w_1$, $w_3$, $w_5$, $w_7$ and $w_9$. The following table of the values of the operators x, y, z and q for each of the five possible vertex weights can be constructed:

| weight | vertex | x | y | z | q |
|---|---|---|---|---|---|
| $w_1$ | u u<br>u u | 1 | 1 | 1 | 1 |
| $w_3$ | u d<br>u d | -1 | 1 | -1 | 1 |
| $w_5$ | d u<br>u d | -1 | -1 | 1 | 1 |
| $w_7$ | d d<br>u u | 1 | -1 | -1 | 1 |
| $w_9$ | d u<br>u u | 0 | 0 | 0 | -1 |

This may not seem to be of much help, but a little consideration shows that linear combinations of x, y, z and q can be formed, such that there is one linear combination which is 1 for a given vertex weight, and zero for all the others. These linear combinations, and the vertices for which they give 1, are

$$\nu_1 = \frac{1}{4}[x + y + z + \frac{1}{2}(1 + q)] \quad \text{for } w_1 = w_2$$

$$\nu_3 = \frac{1}{4}[-x + y - z + \frac{1}{2}(1 + q)] \quad \text{for } w_3 = w_4$$

$$\nu_5 = \frac{1}{4}[-x - y + z + \frac{1}{2}(1 + q)] \quad \text{for } w_5 = w_6$$

$$\nu_7 = \frac{1}{4}[x - y - z + \frac{1}{2}(1 + q)] \quad \text{for } w_7 = w_8$$

$$\nu_9 = \frac{1}{2}(1 - q) \quad \text{for } w_{9\text{-}16} \; . \qquad (8\text{-}17)$$

Then it is easy to see that for $B_z = 0$, the general weight of a vertex composed from arbitrary spins $S_1$, $S_2$, $S_3$ and $S_4$ can be written

$$w_{S_1,S_2,S_3,S_4} = w_1^{\nu_1} w_3^{\nu_3} w_5^{\nu_5} w_7^{\nu_7} w_9^{\nu_9}$$

$$= (w_1 w_3 w_5 w_7 w_9^4)^{1/8} \left(\frac{w_1 w_7}{w_3 w_5}\right)^{x/4} \left(\frac{w_1 w_3}{w_5 w_7}\right)^{y/4} \left(\frac{w_1 w_5}{w_3 w_7}\right)^{z/4} \left(\frac{w_1 w_3 w_5 w_7}{w_9^4}\right)^{q/8} \quad . \quad (8\text{-}18)$$

At this point we can remove the restriction $B_z = 0$. This implies that the weight gets muliplied by a factor $\exp[b_z(S_1+S_2+S_3+S_4)]$. Then the weight of an arbitrary block of four spins can be written as

$$w_{S_1,S_2,S_3,S_4} = \exp[-\beta E_{S_1,S_2,S_3,S_4}] \quad , \quad (8\text{-}19)$$

where

$$E_{S_1,S_2,S_3,S_4} = J_h(S_1S_2 + S_3S_4) + J_v(S_1S_4 + S_2S_3) + J_d(S_1S_3 + S_2S_4)$$

$$+ J_4 S_1S_2S_3S_4 + J_0 - (b_z/\beta)(S_1+S_2+S_3+S_4) \quad . \quad (8\text{-}19b)$$

The coupling constants are complicated functions of the temperature and the Trotter index

$$J_h = (2\beta)^{-1} \ln\left(\frac{w_3 w_5}{w_1 w_7}\right) \quad , \quad \text{horizontal coupling,}$$

$$J_v = (2\beta)^{-1} \ln\left(\frac{w_5 w_7}{w_1 w_3}\right) \quad , \quad \text{vertical coupling,}$$

$$J_d = (2\beta)^{-1} \ln\left(\frac{w_3 w_7}{w_1 w_5}\right) \quad , \quad \text{diagonal coupling,}$$

$$J_4 = 2\beta^{-1} \ln\left(\frac{w_9^4}{w_1 w_3 w_5 w_7}\right) \quad , \quad \text{four spin coupling,}$$

$$J_0 = -(8\beta)^{-1} \ln(w_1 w_3 w_5 w_7 w_9^4) \quad . \tag{8-20}$$

(Note that one must use the $b_z = 0$ weights from (8-14) in these expressions!) Thus we have shown that the 16 vertex model is equivalent to a 2-D Ising model with different nearest neighbor exchange constants in the spatial and Trotter directions, together with a next nearest neighbor diagonal interaction and a four spin coupling. Also recall that this interaction exists only in the shaded boxes of the "checkerboard".

For the 6 and 8 vertex models, the above results are not quite correct. In the 6 vertex model ($B_x = 0$ and $J_x = J_y$), $w_7 = w_9 = 0$, while in the 8 vertex model ($B_x = 0$) only $w_9 = 0$. Consider first the 8 vertex model. Vertices 9 through 16 are always prohibited, and therefore get zero weight. Therefore, in place of the factor $w_9^{\nu_9}$ in equation (8-18), which would be undefined, we must use the factor $(1-\nu_9)$, which can be only zero or 1. Similarly, if $w_7 = 0$, then the factor $w_7^{\nu_7}$ should be replaced by $(1-\nu_7)$. So, for example, in the 8 vertex model the four spin interaction $J_4 S_1 S_2 S_3 S_4$ is replaced by a logarithmic interaction $-\beta^{-1} \ln(\frac{1}{2} + 8S_1 S_2 S_3 S_4)$, which prohibits vertices 9 through 16. For the 8 vertex model, the other exchange constants are no different from those for the 16 vertex model. The zero of energy $J_0$ is, however. Similar modifications can be made to get the effective Hamiltonian for the 6 vertex model; one finds logarithmic four spin and two spin interactions.

For the 8 vertex model, the exchange constants simplify, as do the vertex weights. Putting $B_x = B_z = 0$ in equation (8-14), one has

$$w_1 = e^{K_z} \cosh K_-$$

$$w_3 = e^{-K_z} \cosh K_+$$

$$w_5 = e^{-K_z} \sinh K_+$$

$$w_7 = e^{K_z} \sinh K_-$$

$$w_{9-16} = 0 \quad . \tag{8-21}$$

The 2-D exchange constants are found to be

$$J_h = (2\beta)^{-1} \ell n(e^{-4K_z} \sinh 2K_+ / \sinh 2K_-)$$

$$J_v = (2\beta)^{-1} \ell n(\tanh K_+ \tanh K_-)$$

$$J_d = (2\beta)^{-1} \ell n(\tanh K_- / \tanh K_+)$$

$$J_0 = (8\beta)^{-1} \ell n(\tfrac{1}{4} \sinh 2K_+ \sinh 2K_-) \quad . \tag{8-22}$$

Later we will see that it is useful to choose the xz plane to be the easy plane, so that the applied field ($B_z$) can be in the easy plane for this 8 vertex model. This is shown in Figure 8.1, where the quantization axis is in the easy plane parallel to the field. For the anisotropy believed to describe CHAB (5%, from Kopinga et al. 1984), we can take $J_x = J_z = 1.0$ and $J_y = 0.95$, measuring temperature T in units of 110 K. For these parameters, the 2-D exchange constants are plotted vs. 4mT in

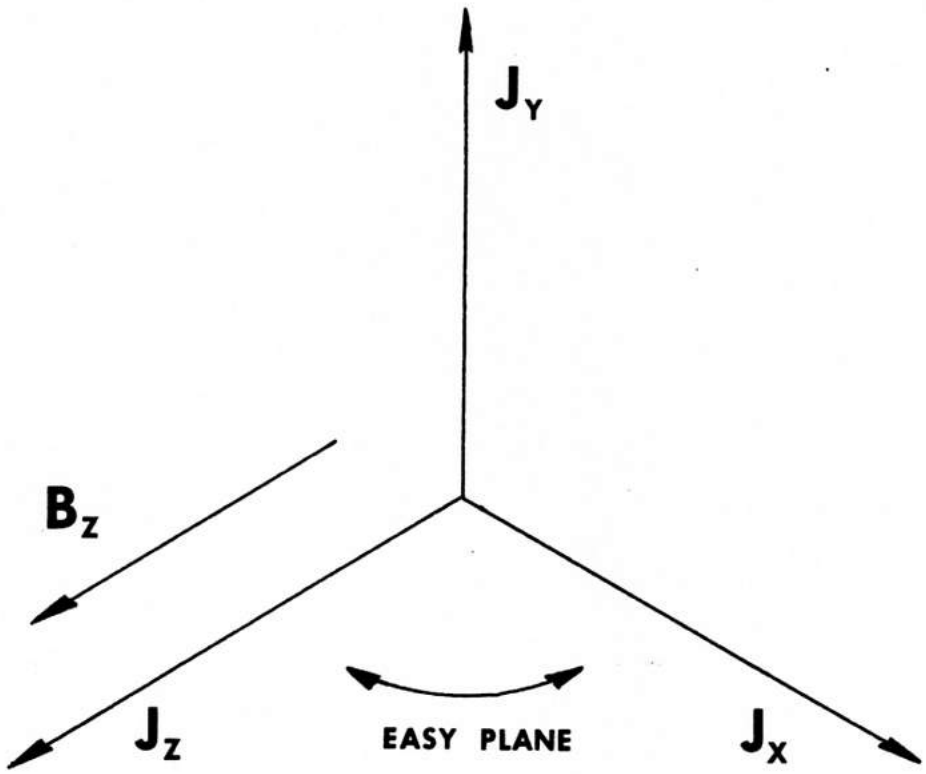


Figure 8.1 The coordinate system for the easy-plane 8 vertex spin-½ model. The applied field, in the easy plane, is parallel to the quantization axis.

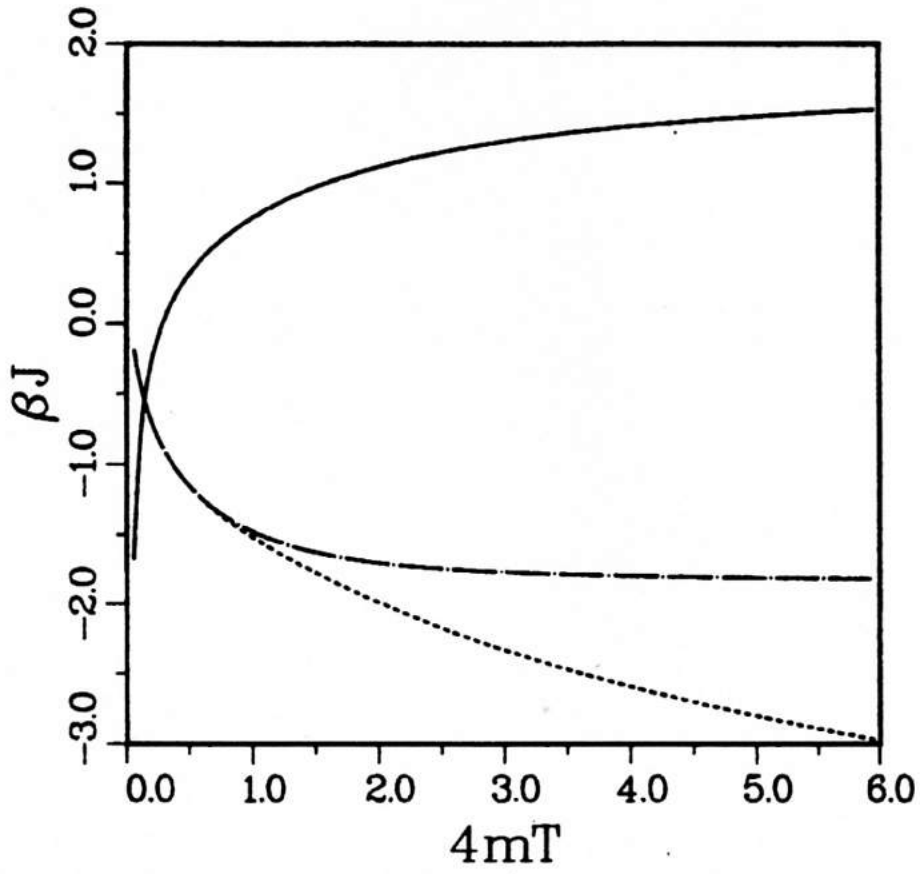


Figure 8.2 The effective exchange constants on the 2-D lattice for the 8 vertex spin ½ easy-plane model, with $J_x = J_z = 1.0$, $J_y = 0.95$. The solid curve is $\beta J_h$, the spatial coupling, the dashed curve is $\beta J_v$, the coupling in the Trotter direction, and the chain curve is $\beta J_d$, the diagonal coupling, where $\beta = 1/k_B T$. The spatial coupling is antiferromagnetic except at very low temperatures, even though the original 1-D quantum model has only ferromagnetic coupling.

Figure 8.2. At extremely low T, all three are negative (ferromagnetic). However, there is a temperature above which $J_h$ becomes positive (antiferromagnetic), and the 2-D classical system has competing ferromagnetic and antiferromagnetic interactions. This may have the effect of generating metastable nonequilibrium trajectories in the Monte Carlo calculations, which could affect the efficiency of a given algorithm.

## 8.3 Spin Flipping Algorithms for the 6, 8 and 16 Vertex Models

In principle, the simplest model to work with is the 16 vertex model, since individual spin flips can be the basic Monte Carlo moves (a single spin flip leads to another allowed state). In the 8 vertex model, one must always flip the spins in a vertex in pairs to generate another allowed vertex, and this necessitates flipping a series of spins in the 2-D lattice that lie on a closed path. Then the basic moves can be column, row and square flips as used by Cullen and Landau (1983). We could also use their staggered column flips, but is seems that they can always be decomposed into a series of square flips plus one column flip, and so they are not necessary. In the 6 vertex model, we do not know a simple set of moves which keeps one within the 6 allowed vertices, so that a combination of column, row and square flips can generate disallowed states and waste computing time. Ironically the presence of too much symmetry in the original Hamiltonian makes the case of isotropic exchange with only a field parallel to the quantization axis the most difficult in this formalism.

Initially the 16 vertex model was applied to CHAB, for which the parameter values are believed to be $J_x = J_y = 110$ K, $J_z = 104.5$ K (Kopinga et al. 1982, 1984). For fields $B_z = 0$ and $0 \leq B_x \leq 10$kG, one finds that

the percentage of single spin flips accepted using the standard Metropolis et al. (1953) algorithm is impractically small, less than 1% for $1\ K \leq T \leq 10\ K$. This is because this model is approximately a 6 vertex model, with the magnetic field just a mild perturbation. The 16 vertex model works well only if the field, exchange constants and temperature are all the same order of magnitude. A single spin flip in a vertex causes a transition from a vertex with an odd (even) number of $+\frac{1}{2}$'s to a vertex with an even (odd) number of $+\frac{1}{2}$'s. When the field is small compared to the exchange, vertices with an odd number of $+\frac{1}{2}$'s have energies much larger than the other vertices, and single spin flip acceptance rates rapidly approach zero as the field does. This is the major source of difficulty with this 16 vertex model. It is especially important to have a formalism where the field can be set to zero, since usually the zero field specific heat is subtracted from the specific heat with field to test the sG ideal gas theory. (This removes the specific heat contribution from linear spin waves.)

Therefore it is better to consider an 8 vertex model. To obtain an 8 vertex model to apply to CHAB, we should orient the coordinate system as shown in Figure 8.1, taking $J_x = J_z = 110\ K$, and $J_y = 104.5\ K$, with $B_x = 0$, $0 \leq B_z \leq 10\ kG$. Now the quantization axis lies in the easy plane parallel to the field, and the model remains an 8 vertex model even when the field goes to zero. Obviously, though, if there is no easy-plane anisotropy, then this model degenerates back to the 6 vertex model. So we require adequate anisotropy for this model to work efficiently using a combination of row, column and square flips. This is the model for which we have performed the Monte Carlo calculation. Some of these results have already been reported in Satija et al. (1985).

## 8.4 Monte Carlo Details

Details of the Monte Carlo procedure are briefly described. In a single Monte Carlo step, we attempt N column flips and $\frac{1}{2}$Nm square flips, chosen at random positions in the lattice. Row flips usually have very low acceptance rates and so have not been used. If all of these flips are accepted, then each spin in the lattice would be flipped twice on average, once via a column flip and once via a square flip. Of course only a small fraction (~ 10%) is usually accepted. After one of these steps, data is then stored for the expectation values to give $\langle F_k \rangle$, $\langle G_k \rangle$, and so on for the thermodynamic functions. Typical calculations used from $10^5$ to $3 \times 10^5$ steps, with the first 20% discarded, and the rest divided into $\simeq$ 10 groups for error analysis. We computed the appropriate expectation values to get the internal energy, specific heat, magnetization and susceptibility as described by Cullen and Landau (see section 7.3). The algorithm has been partially checked by comparison with an exact m = 1 transfer matrix calculation.

The system was started in some standard initial configuration, such as alternating up and down spins in each row and column. Then a number of Monte Carlo steps ($\simeq$ 3000) was taken at twice the desired temperature to "heat up" or "stir" the system. The temperature was then set back to the desired value, the vertex energies recalculated, since they depend on temperature, and the calculations were then begun. The data obtained using several such initial states was averaged to produce the results shown here. Calculations were performed for no field, and $B_z$ = 3.3 kG, 6.5 kG and 10.0 kG in order to compare with available experimental data. We have used N = 32 and m = 2,4,6,8,12 and 16. For the present case, it seems that the choice m = 8 is the optimum for which the statistical errors are about the same size as the errors due to using the finite m

Trotter approximation ($\lesssim$ 5% for the statistical errors). Generally statistical errors increase with m, unless the number of Monte Carlo steps is greatly increased, while the Trotter errors decrease with m.

Results for CHAB are shown in Figure 8.4, for m = 8, N = 32. Also the m = 4 and m = 12 CHAB results are shown in Figures 8.3 and 8.5. Before a discussion and comparison to the experimental data, we describe next the prediction of the sG phenomenlogical theory, particularly for the classical soliton contribution to the specific heat.

## 8.5 Sine-Gordon Soliton Gas Thermodynamics

The phenomenological theory of the thermodynamics of a gas of sG solitons and linear classical phonons (spin waves in the present context) has been presented by Currie et al. (CKBT, 1980). This theory stemmed from the earlier work of Krumhansl and Schrieffer (1975). The theory will not be reviewed here, rather, we will use only some specific results from it, which can be applied to both CHAB and $CsNiF_3$.

CKBT have determined the effect of a low density gas of sG solitons on the free energy of the linear modes in thermodynamic equilibrium, where the dynamics is governed by the sG equation. The change in the free energy is attributed to the presence of the sG solitons, and thus they have obtained an expression for the soliton contribution to the free energy. (Breathers are a higher order effect.) The free energy density $F_{tot}$ (free energy per particle) is given to leading order as the sum of spin wave ($F_{sw}$) and soliton contributions ($F_k$),

$$F_{tot} = F_{sw} + F_k \tag{8-23a}$$

$$F_{sw} = (2\pi\beta)^{-1} \int_{-\pi}^{\pi} dk \; \ell n(\beta\hbar\omega_k) \tag{8-23b}$$

$$F_k = -\beta^{-1}\, n_k^{tot} \quad . \tag{8-23c}$$

The spin wave dispersion relation, for a discrete lattice, is found to be (in this sG limit of the equations of motion)

$$\bar{\alpha}\omega_k^2 = \beta_f + 4\,\sin(\tfrac{1}{2}k) \tag{8-24a}$$

where

$$\bar{\alpha} \equiv 2A/J \qquad \beta_f \equiv g\mu_B B_z/JS \quad . \tag{8-24b}$$

A and J are the parameters for the classical Hamiltonian; in the case we can make the approximations $J = J_x = J_z$, $A = J_x - J_y$, using the coordinates of Figure 8.1. The sG soliton free energy is directly proportional to the total number density per unit length of solitons and antisolitons $n_k^{tot}$, given by

$$n_k^{tot} = \frac{2}{w_0}\left(\frac{2\beta E_0}{\pi}\right)^{\frac{1}{2}} e^{-\beta E_0} \quad . \tag{8-25}$$

$E_0$ and $w_0$ are the static soliton energy and width,

$$E_0 = 8(g\mu_B B_z JS^3)^{\frac{1}{2}} \quad , \quad w_0^2 = JS/g\mu_B B_z = \beta_f^{-1} \tag{8-26}$$

Note that equations (8-23c) and (8-25) are valid only in the low temperature limit (low number density of mildly interacting solitons), $\beta E_0 \gg 1$. In this limit, the internal energy density U and the specific heat per unit length C are given from derivatives of $F_{tot}$,

$$U = \frac{\partial}{\partial\beta}(\beta F_{tot}) = k_B T + (E_0 - \tfrac{1}{2}k_B T)n_k^{tot} \tag{8-27}$$

$$C = \frac{\partial U}{\partial T} = k_B + [(E_0/k_B T - \tfrac{1}{2})^2 - \tfrac{1}{2}]k_B n_k^{tot} \tag{8-28}$$

The first term in each of these expressions is the linear spin wave contribution; the second term is the soliton-antisoliton contribution. In both cases the spin wave contribution is indepedent of the applied field; thus the reason for presenting results where the zero field specific heat (or internal energy) has been subtracted from the result with a field. This should remove the spin wave contribution. Similarly, the magnetization can be found as the sum of spin wave and soliton contributions, $M_{sw}$ and $M_k^{tot}$, and the ground state value $M_0$,

$$M_z = - \frac{\partial F_{tot}}{\partial B_z} = M_0 + M_{sw} + M_k^{tot} \tag{8-29a}$$

$$M_0 = g\mu_B S \tag{8-29b}$$

$$M_{sw} = - \frac{1}{4} \frac{k_B T}{JS^2} (\beta_f + 4)^{-\frac{1}{2}} M_0 \tag{8-29c}$$

$$M_k^{tot} = \frac{1}{2} n_k^{tot} w_0^2 (\frac{3}{2} - \beta E_0) \frac{\beta M_0}{JS^2} \quad . \tag{8-29d}$$

One further derivative with respect to the field gives the susceptibility continues $\chi_{sw}$ and $\chi_k^{tot}$

$$\chi_{sw} = \frac{1}{8} k_B T \left( \frac{M_0}{JS^2} \right)^2 (\beta_f + 4)^{-3/2} \tag{8-30a}$$

$$\chi_k^{tot} \simeq 16\beta^3 n_k^{tot} w_0^2 M_0^2 \quad . \tag{8-30b}$$

It will make sense to apply these formula only for $\beta E_0 \gg 1$. For the CHAB parameters $S = \frac{1}{2}$, $J = 110$ K, $g = 2.0$, and considering fields $B_z =$ 3.3, 6.5 and 10.0 kG, the rest energy of the solitons is $E_0 = 20$, 28 and

34 K respectively ($E_0 = 10.87\ B^{1/2}$, $E_0$ in K, B in kG). Therefore the sG phenomonological theory can be used only well below these temperatures, at these fields. For $CsNiF_3$, the parameters are S = 1, J = 23.6 K and g = 2.4, and for fields $B_z$ = 3.0, 5.0 and 10.0 kG, the soliton rests energies are $E_0$ = 27, 35 and 49 K respectively ($E_0 = 15.6\ B^{1/2}$). Then these are the limiting temperatures for which the sG theory can be applied to $CsNiF_3$.

## 8.6 Results for CHAB

Results from the Monte Carlo calculation for CHAB at four different fields $B_z$ are shown in Figures 8.3, 8.4 and 8.5 for m = 4, 8 and 12 respectively. All results shown are for a system of 32 spins with periodic boundary conditions. For the fields 3.3, 6.5 and 10.0 kG used, the soliton full-widths are 22, 16 and 12 lattice units respectively, each less than the system size. We show the internal energy, specific heat, magnetization and susceptibility in each case. In Figure 8.6 the difference $\Delta C = C(B_z) - C(0)$ is plotted vs. T, and can be compared with the experimental results of Kopinga et al. (1984) shown in Figure 8.7.

The Monte Carlo results for $\Delta C$ are in fair agreement with the experimental data regarding the temperature at which $\Delta C$ maximizes. The most obvious differences are a tendency for the Monte Carlo results to lie below the experimental ones by about 20%. There are several possible explanations: i) There could be a systematic additional specific heat component measured experimentally, for example, nonmagnetic contributions (perhaps spin wave-acoustic wave coupling) or entropy-reducing pinning effects in the absence of the field, ii) The assumed Hamiltonian may not be appropriate, either because of errors in the assumed parameter values, or corrections to the assumed form of the interactions. Generally the

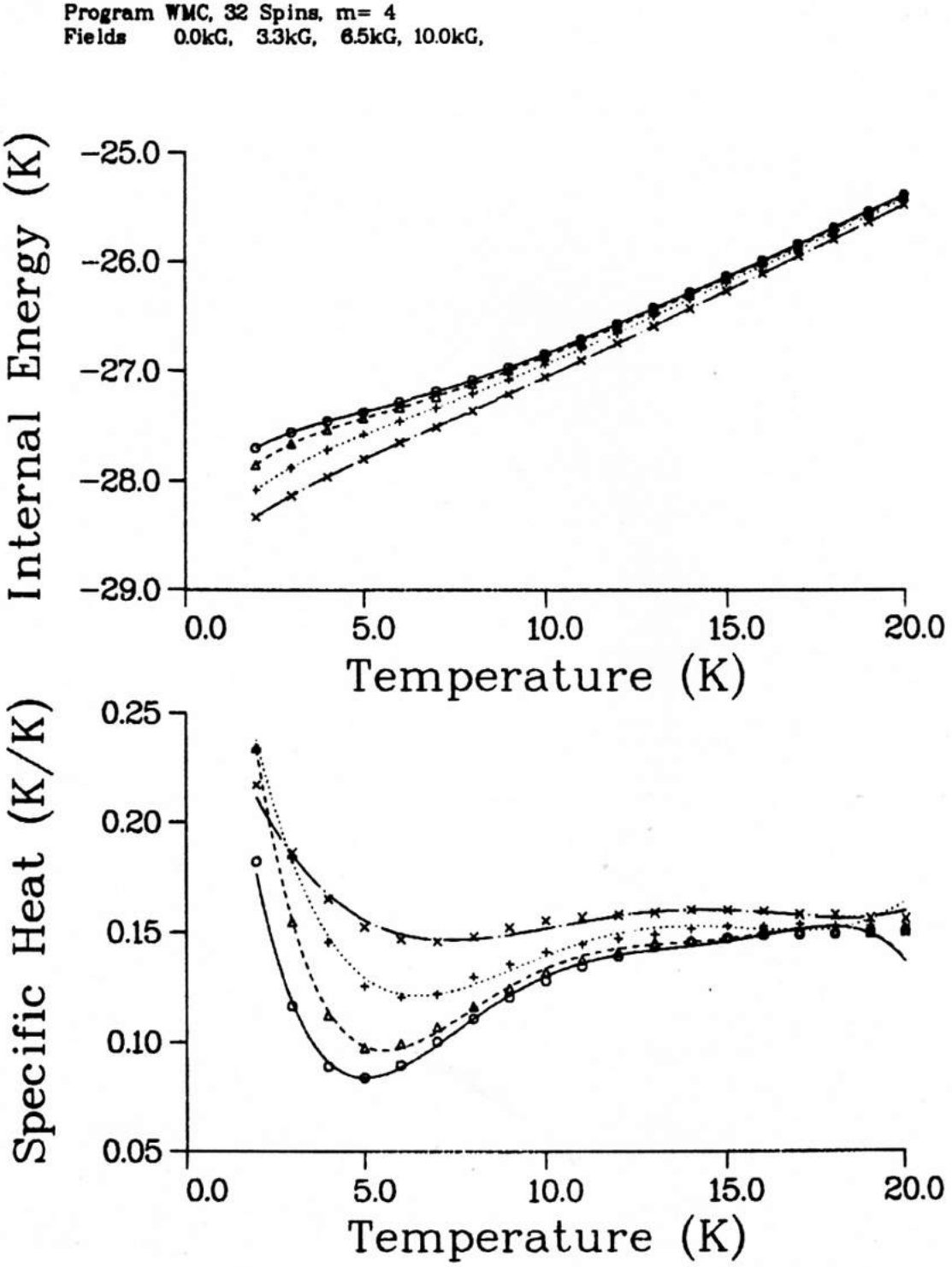


Figure 8.3a Monte Carlo results for CHAB, with m = 4, at fields $B_z$ = 0.0 (0), 3.3 (Δ), 6.5 (+) and 10.0 (x) kG. The data points are from the opposite Monte Carlo expectation values. The curves for the internal energy are weighted least square polynomial fits to the data points, while the curves for the specific heat are the derivatives of those polynomials fits.

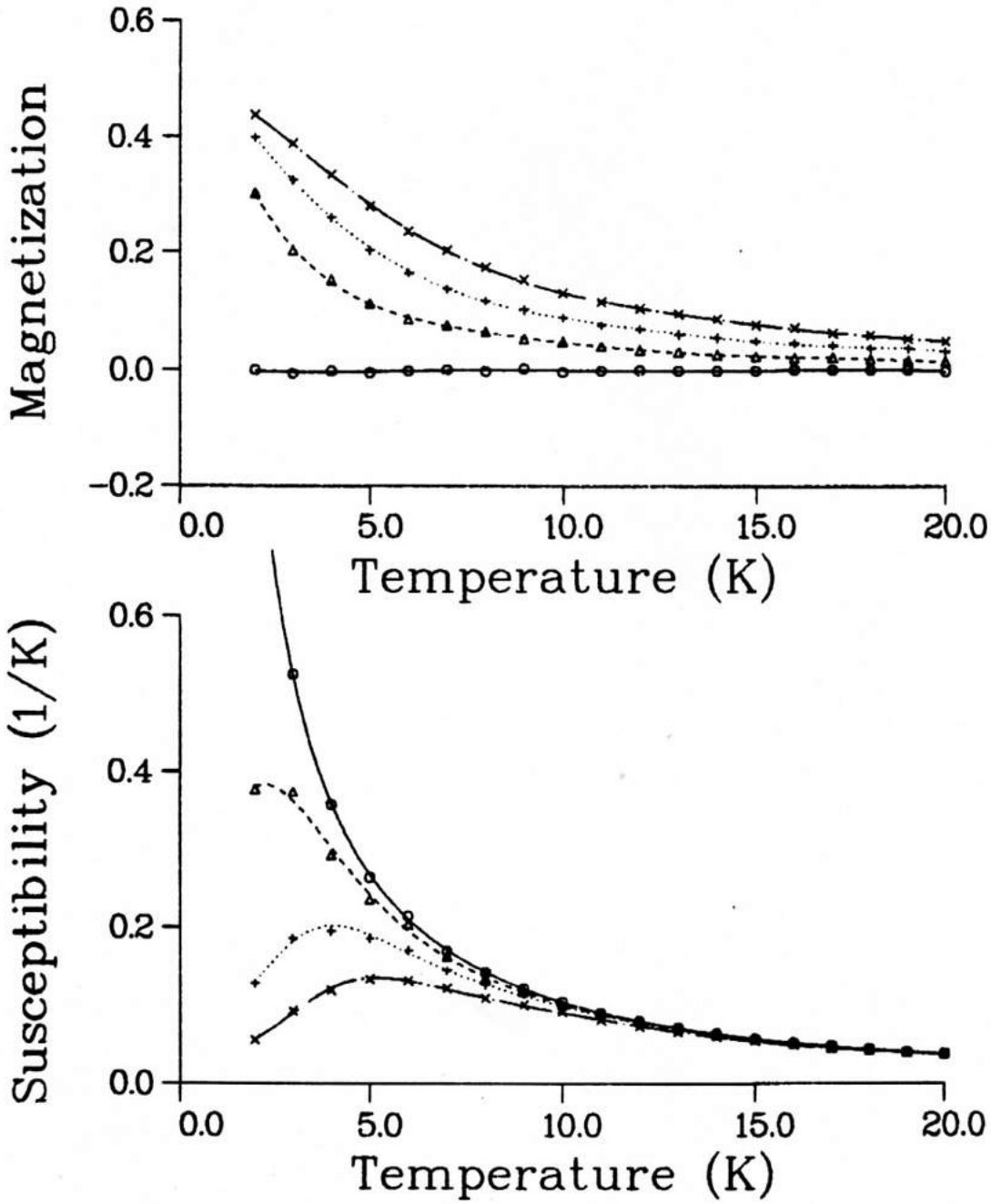


Figure 8.3b Monte Carlo results for CHAB, with m = 4, at fields $B_z$ = 0.0 (0), 3.3 (Δ), 6.5 (+) and 10.0 (x) kG. The data points are from the appropriate Monte Carlo expectation values. The curves are weighted least square polynomial fits to the data points.

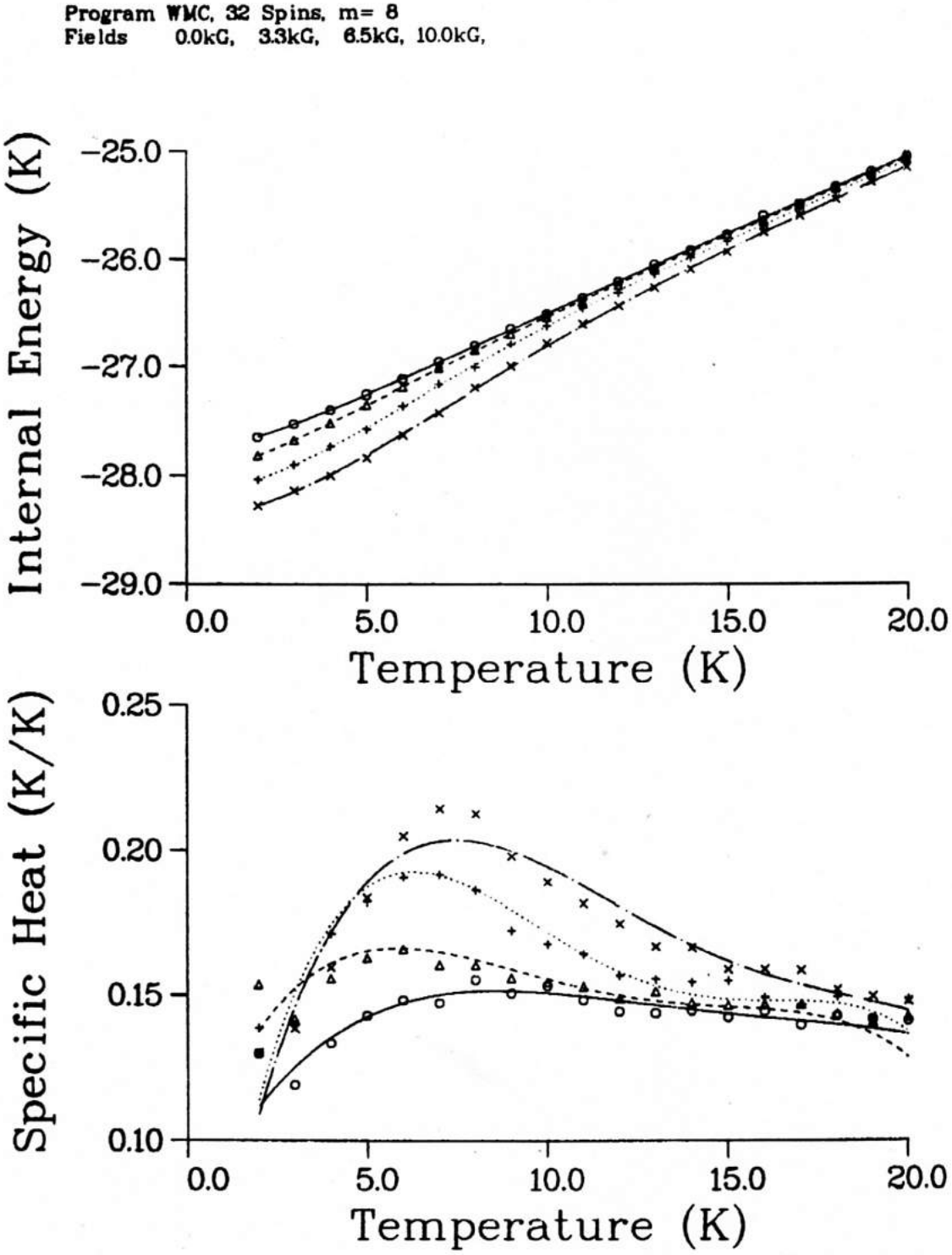


Figure 8.4a Monte Carlo results for CHAB, with m = 8, at fields $B_z$ = 0.0 (0), 3.3 (Δ), 6.5 (+) and 10.0 (x) kG. The data points are from the appropriate Monte Carlo expectation values. The curves for the internal energy are weighted least square polynomial fits to the data points, while the curves for the specific heat are the derivatives of those polynomial fits.

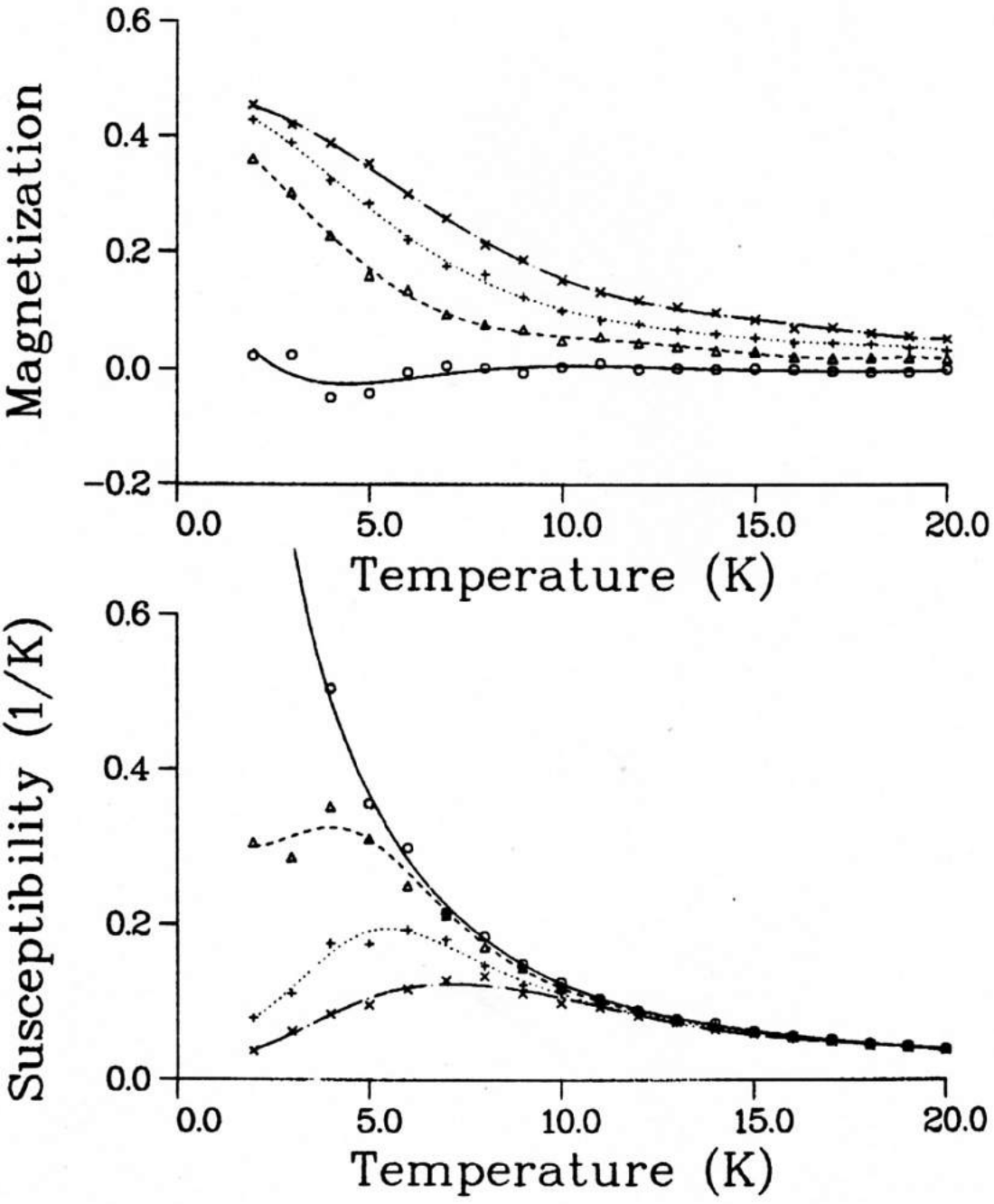


Figure 8.4b Monte Carlo results for CHAB, with m = 8, at fields $B_z$ = 0.0 (0), 3.3 (Δ), 6.5 (+) and 10.0 (x) kG. The data points are from the appropriate Monte Carlo expectation values. The curves are weighted least square polynomial fits to the data points.

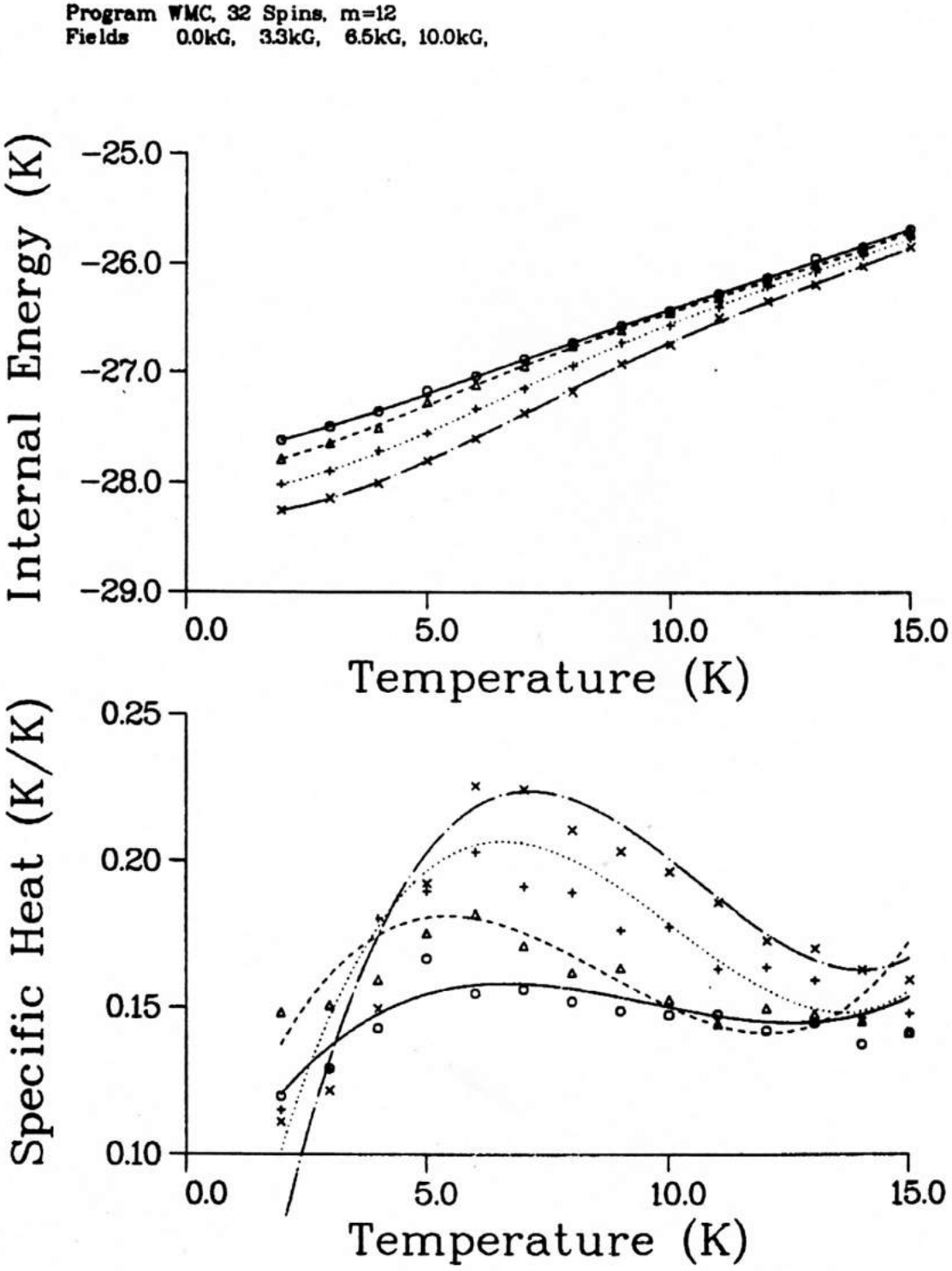


Figure 8.5a Monte Carlo results for CHAB, with m = 12, at fields $B_z$ = 0.0 (0), 3.3 (Δ), 6.5 (+) and 10.0 (x) kG. The data points are from the opposite Monte Carlo expectation values. The curves for the internal energy are weighted least square polynomial fits to the data points, while the curves for the specific heat are the derivatives of those polynomials fits.

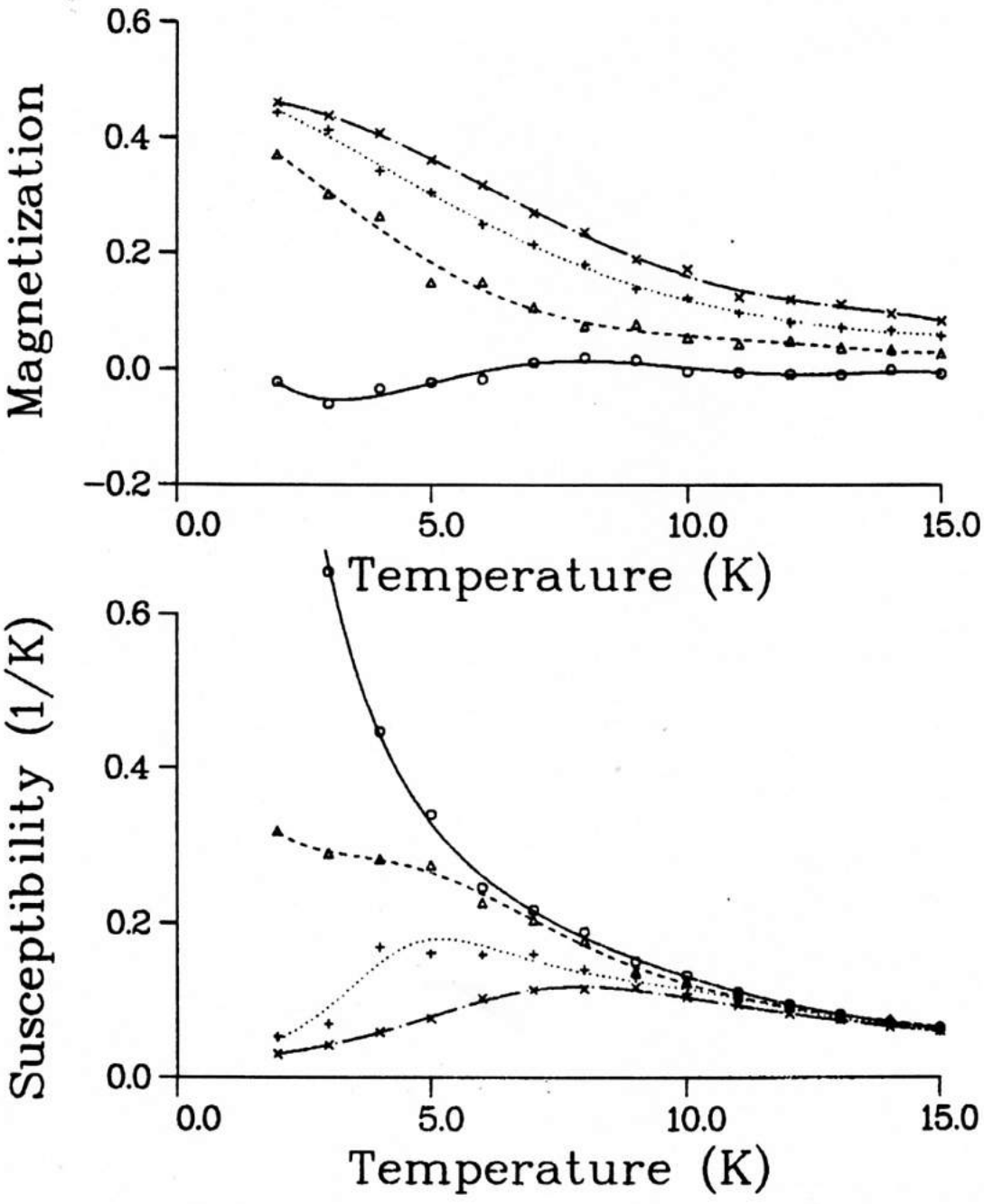


Figure 8.5b Monte Carlo results for CHAB, with m = 12, at fields $B_z$ = 0.0 (0), 3.3 (Δ), 6.5 (+) and 10.0 (x) kG. The data points are from the appropriate Monte Carlo expectation values. The curves are weighted least square polynomial fits to the data points.

Figure 8.6 The differences $\Delta U = U(B_z) - U(0)$, $\Delta C = C(B_z) - C(0)$, from the quantum Monte Carlo, at fields $B_z$ = 3.3 ($\Delta$), 6.5 (+) and 10.0 (x) kG, for (a) m = 4, (b) m = 8 and (c) m = 12. Errors due to the finite m Trotter approximation make the low-T m = 4 results invalid. For larger m, however, the efficiency of the algorithm decreases, and statistical errors increase greatly unless the length of the simulation is adequately increased.

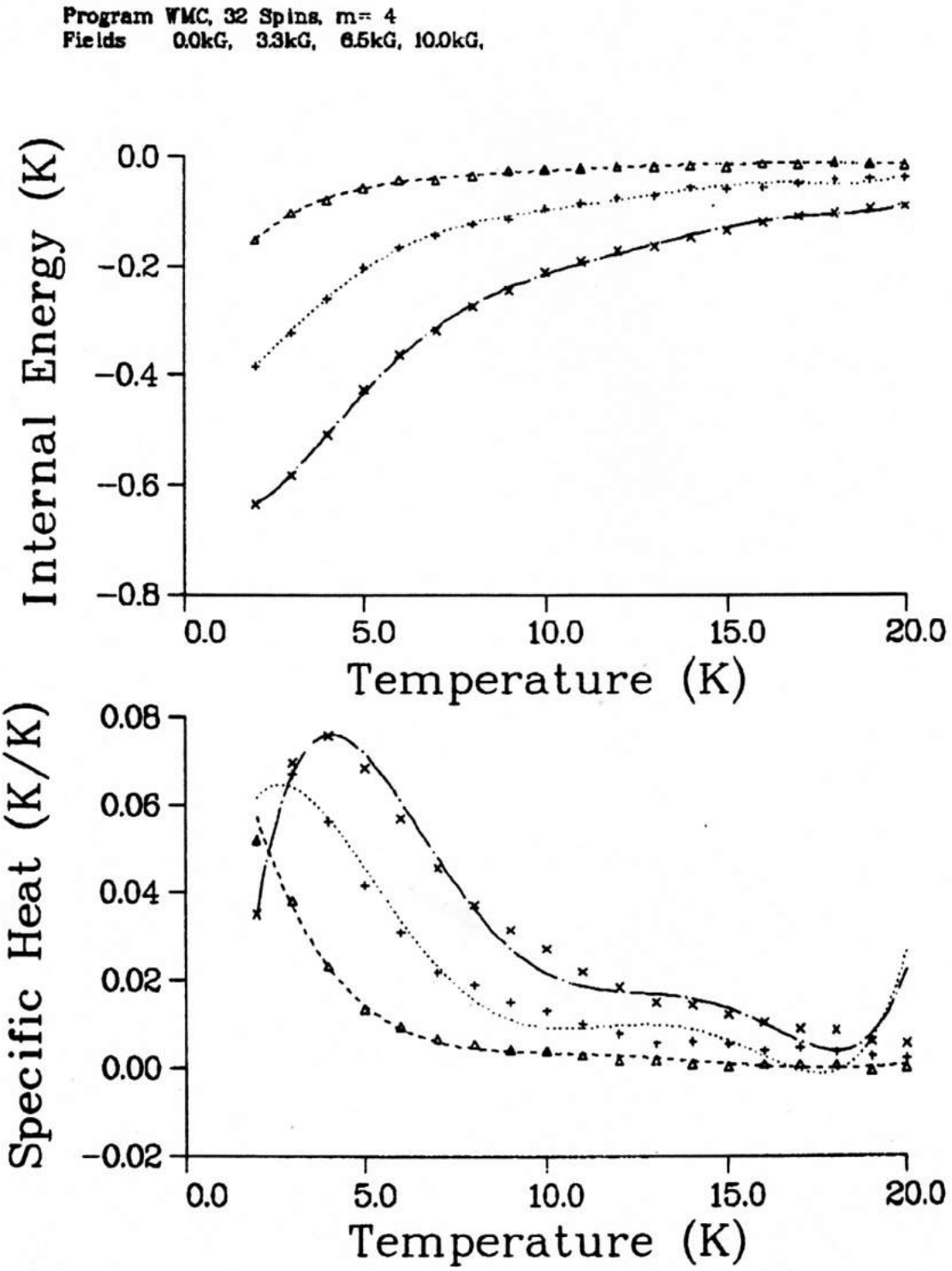
Program WMC, 32 Spins, m= 4
Fields 0.0kG, 3.3kG, 6.5kG, 10.0kG,
Internal Energy (K)
0.0
-0.2
-0.4
-0.6
-0.8
0.0
5.0
10.0
15.0
20.0
Temperature (K)
Specific Heat (K/K)
0.08
0.06
0.04
0.02
0.00
-0.02
0.0
5.0
10.0
15.0
20.0
Temperature (K)

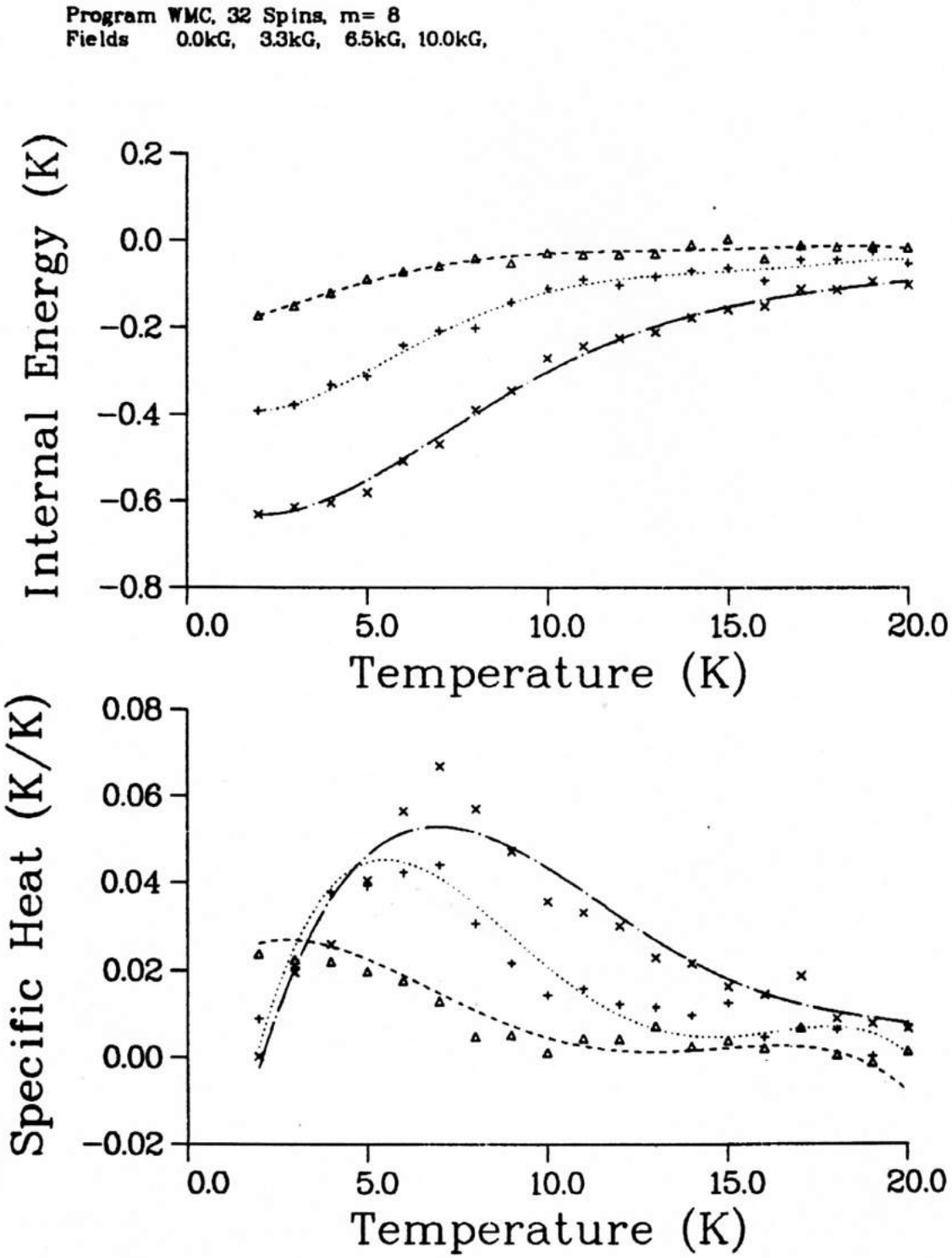
Program WMC, 32 Spins, m= 8
Fields 0.0kG, 3.3kG, 6.5kG, 10.0kG,
Internal Energy (K)
0.2
0.0
-0.2
-0.4
-0.6
-0.8
0.0
5.0
10.0
15.0
20.0
Temperature (K)
Specific Heat (K/K)
0.08
0.06
0.04
0.02
0.00
-0.02
0.0
5.0
10.0
15.0
20.0
Temperature (K)

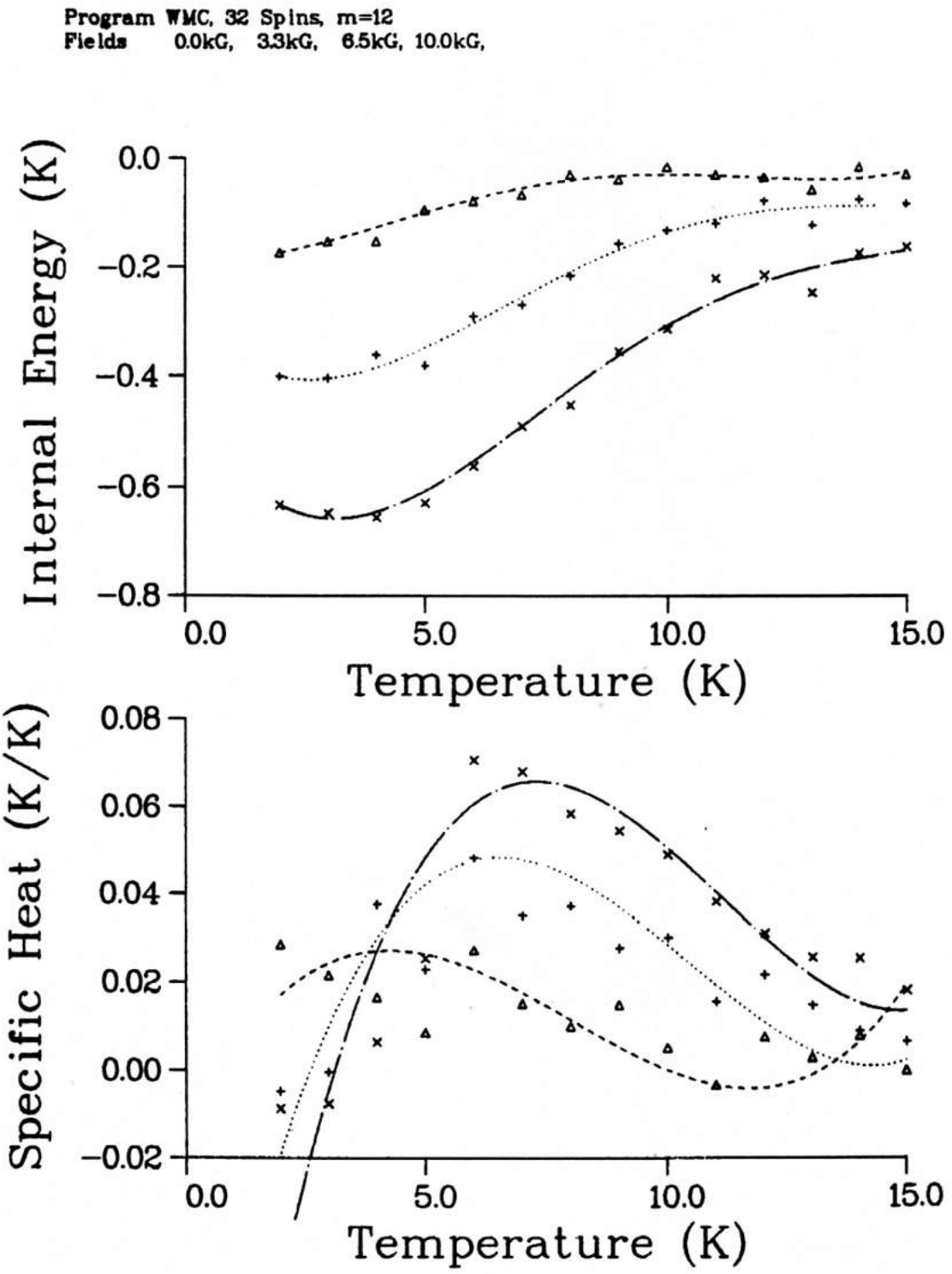
Program WMC, 32 Spins, m=12
Fields 0.0kG, 3.3kG, 6.5kG, 10.0kG,
Internal Energy (K)
0.0
−0.2
−0.4
−0.6
−0.8
0.0
5.0
10.0
15.0
Temperature (K)
Specific Heat (K/K)
0.08
0.06
0.04
0.02
0.00
−0.02
0.0
5.0
10.0
15.0
Temperature (K)

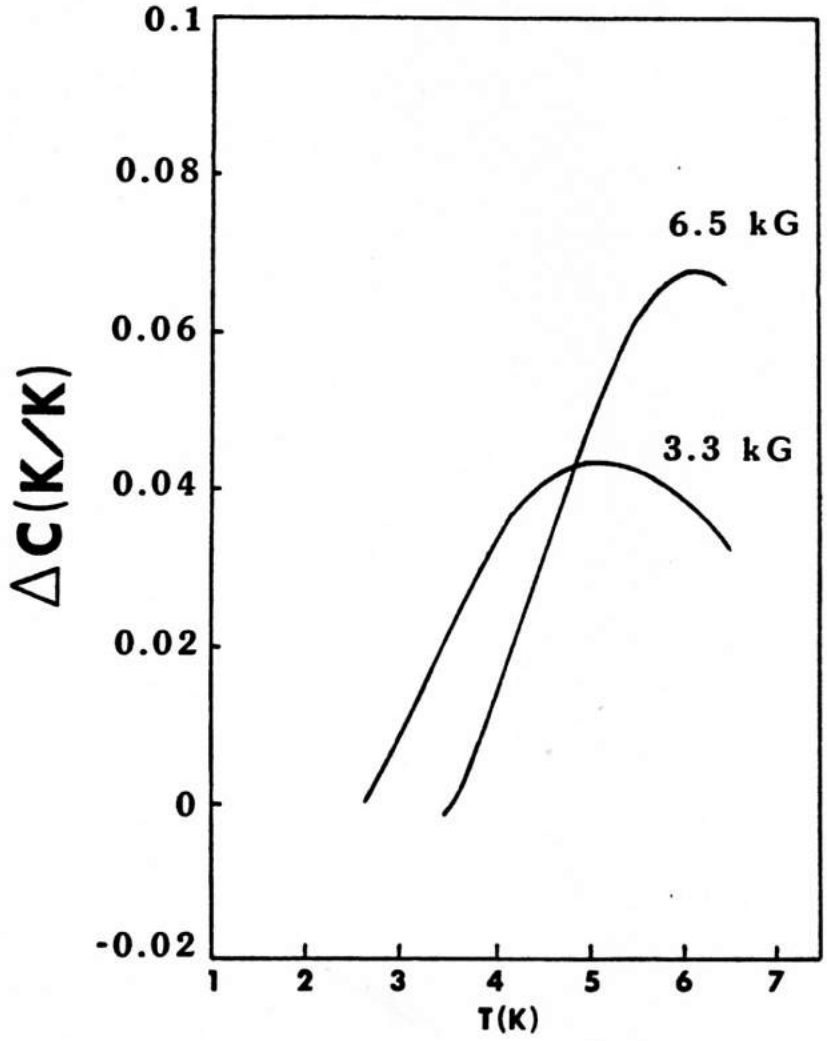


Figure 8.7 Experimental results for ΔC from Kopinga et al. (1984), at fields $B_z$ = 3.3 (Δ) and 6.5 (+) kG. These data fall between the quantum Monte Carlo results and the sG phenomenological results.

parameters $J_x$, $J_y$ and $J_z$ have been determined from fits to linear properties. There is a possibility that more accurate assignments of parameters are necessary before precise comparisons with classical or quantum soliton theories can be made. We have tested the effect of varying the easy plane anisotropy from 3% to 7% (5% was the assumed value). Results for C and $\Delta C$, with m = 8, N = 32, are shown in Figure 8.8 for anisotropies 3%, 5% and 7% at $B_z$ = kG. It is seen that decreasing the anisotropy decreases C, but any systematic changes in $\Delta C$ are small, less than the $\lesssim \pm 15\%$ errors bars for $\Delta C$; iii) Finally, there may be systematic quantum Monte Carlo errors leading to an underestimate of C and $\Delta C$, especially due to using the finite m Trotter approximation, and a finite lattice of size N. There could also be a bias in the spin flipping algorithm; we cannot be sure that all microstates of the system are a priori equally probable in the present method. Possibly these questions could be answered through the use of exact transfer matrix calculations. Some efforts in this direction have been made by this author, but the large size of the applicable transfer matrix causes numerical difficulties.

Finally, for comparison, the thermodynamic results from the sG phenomenological theory are shown in Figure 8.9, using the expressions from section 8.5, with no adjustment of the soliton rest mass. The positions of the peaks in $\Delta C$ vs. T at fixed field occur at larger temperatures than either the Monte Carlo data or the experimental results. A better fit of the sG theory to the experimental data can be obtained, according to Kopinga et al. (1984), by adjusting the soliton energy by a factor of 0.774. This renormalization of the rest energy was obtained by fitting the positions of the peaks in $\Delta C$ vs. $B_z$ at fixed temperature to the prediction of the sG theory for those peak positions, which is

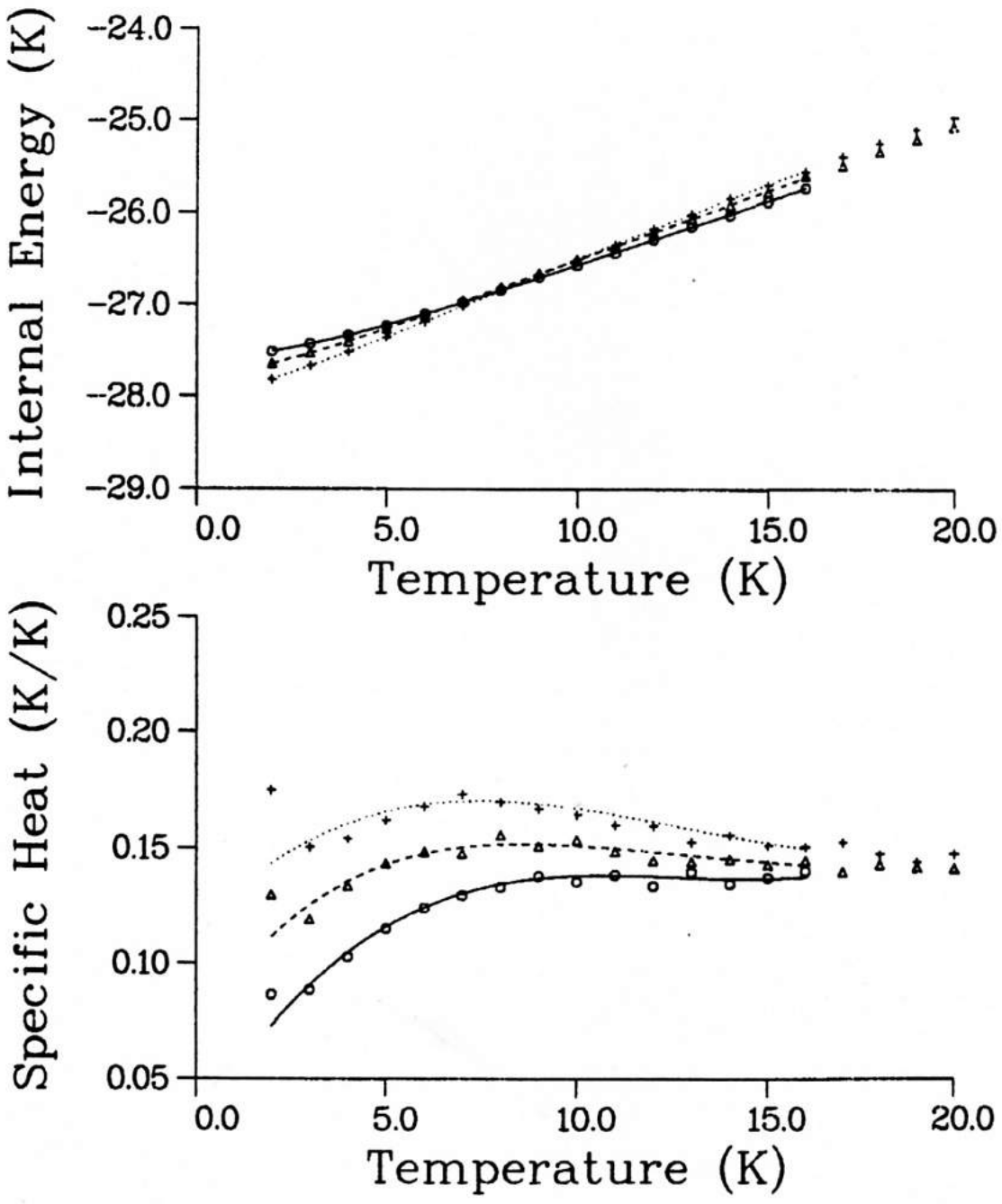


Figure 8.8a Effect of varying the anisotropy $(J_x - J_y)/J_x$ on U and C, at zero field. The curves are for 3% (0), 5% (Δ) and 7% (+) anisotropy, with m = 8.

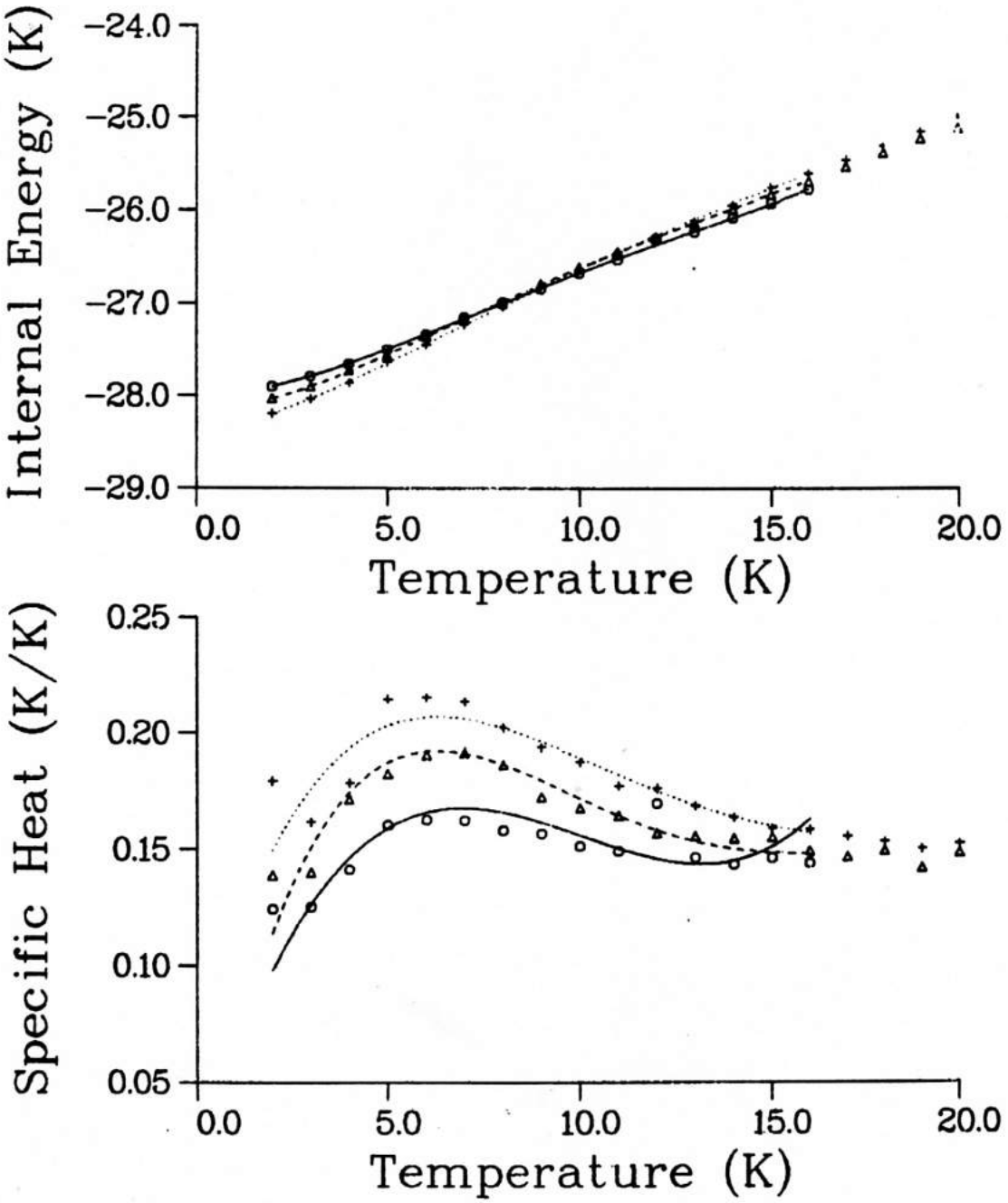


Figure 8.8b Effect of varying the anisotropy $(J_x - J_y)/J_x$ on U and C, at 6.5 kG. The curves are for 3% (0), 5% (Δ) and 7% (+) anisotropy, with m = 8.

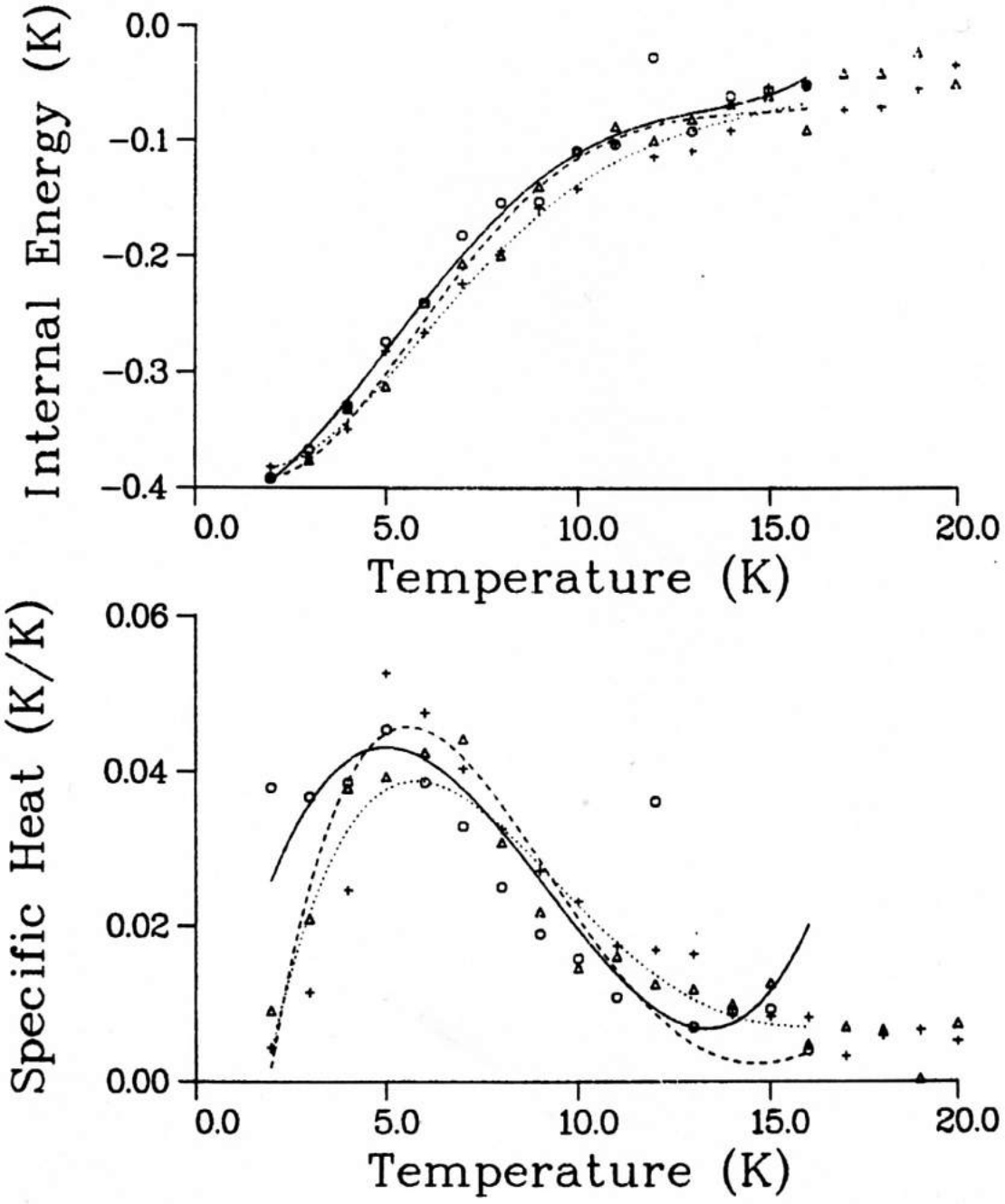


Figure 8.8c Effect of varying the anisotropy on $(J_x - J_y)/J_x$ on $\Delta U$ and $\Delta C$, at 6.5 kG, for 3% (0), 5% (Δ) and 7% (+) anisotropy. Any systematic variation in the peak height or position is difficult to discern.

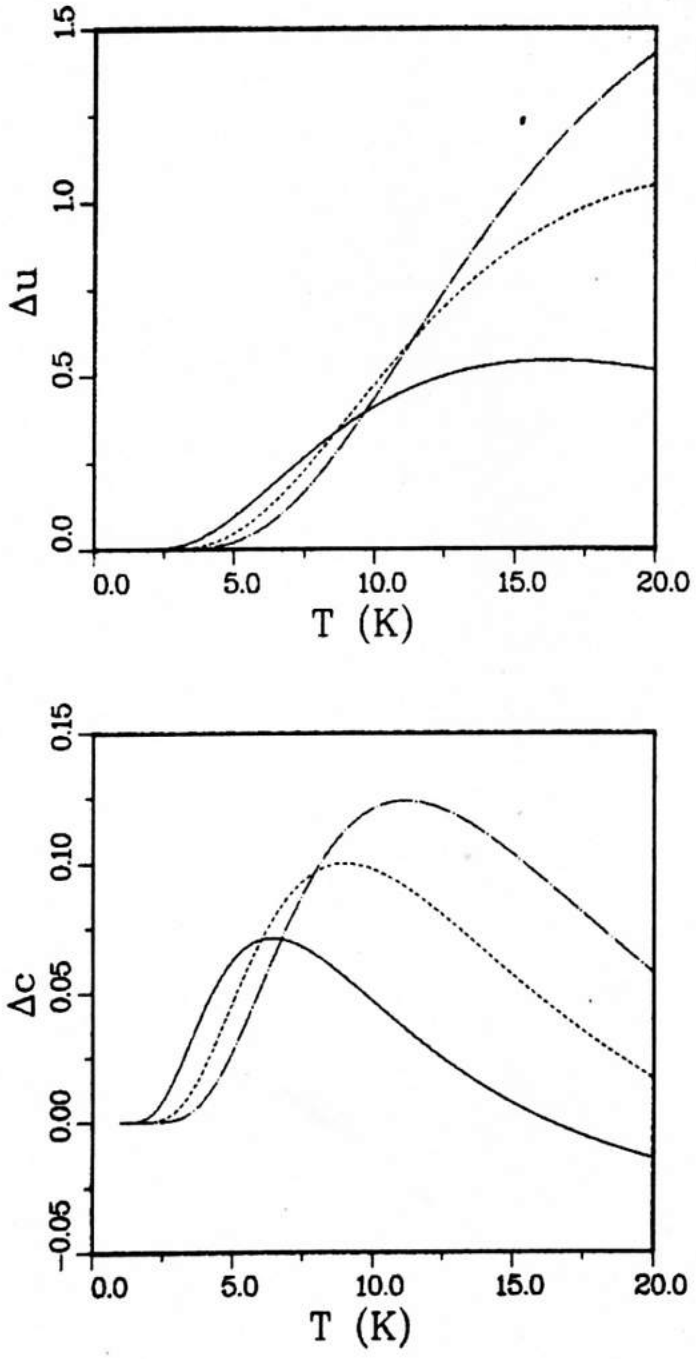


Figure 8.9a sG ideal gas results for ΔU and ΔC, in K and K/K respectively, with no adjustment of the soliton energy, for fields 3.3 (solid), 6.5 (dashed) and 10.0 (chained)kG.

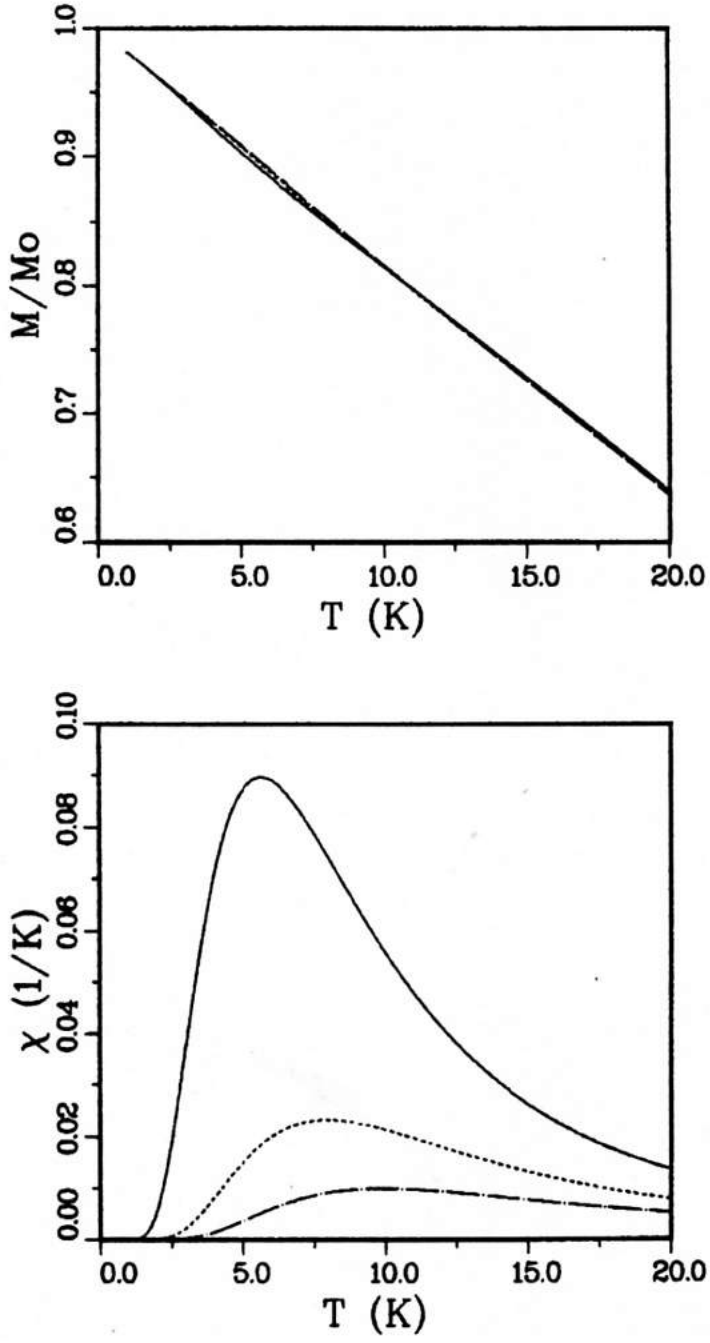


Figure 8.9b sG ideal gas results for M and $\chi$, measured in units of $M_0$ and $M_0^2$ respectively, with no adjustment of the soliton energy, for fields 3.3 (solid), 6.5 (dashed) and 10.0 (chained) kG.

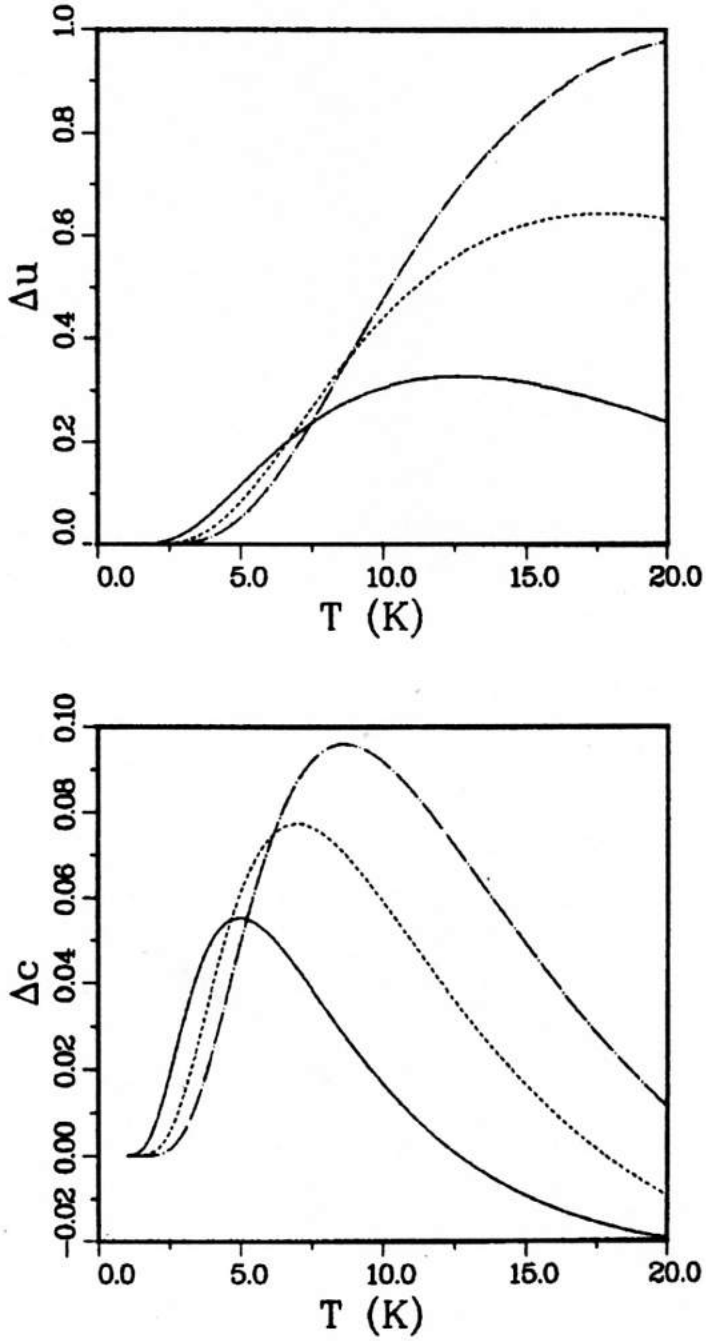


Figure 8.10a sG idea gas results for ΔU and ΔC, using a reduced soliton rest energy E' = .774 $E_0$, for fields 3.3 (solid), 6.5 (dashed) and 10.0 (chained) kG. The peak positions are in close agreement with experiment and the Monte Carlo results, but the peak heights are too high.

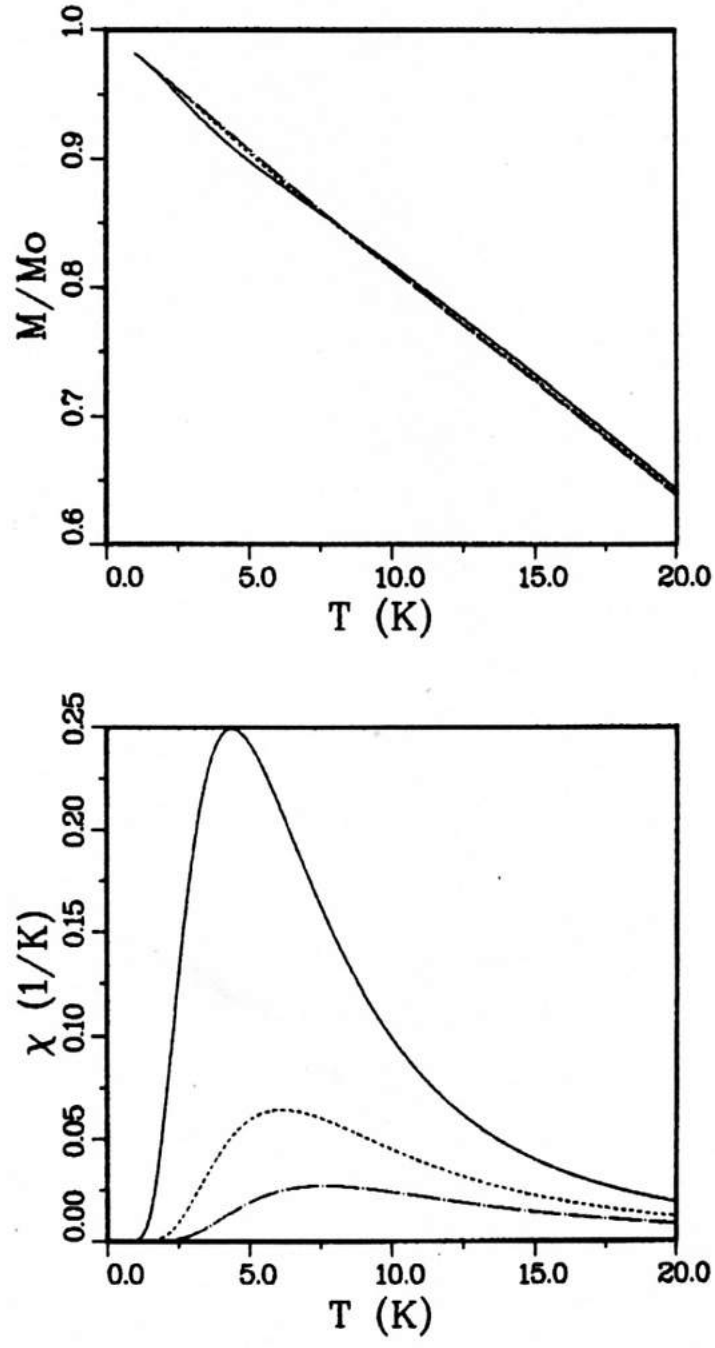


Figure 8.10b sG ideal gas results for M and $\chi$ using a reduced soliton rest energy E' = .774 $E_0$, for fields 3.3 (solid), 6.5 (dashed) and 10.0 (chained) kG.

$$E_0/k_BT = 3.898 \quad . \tag{8-31}$$

$E_0$ depends on the field, in pure sG theory, through

$$E_0 = 8(JS^3\ g\mu_B B_z)^{1/2} = \alpha B_z^{1/2} \quad . \tag{8-32}$$

Combining these equations, the sG theory predicts a quadratic relation between the peak position and temperature

$$B_{peak} = (3.898\ k_BT/\alpha)^2 \quad . \tag{8.33}$$

However, the experimental data give $\alpha$ reduced from the sG prediction by the factor 0.774, which is interpreted as a reduction of the sG rest energy by the same factor. If one re-calculates the internal energy, specific heat, and so on, using this reduced soliton rest mass, the curves of Figure 8.10 result. It is seen that then the peak positions in $\Delta C$ vs. T at fixed field, as derived from Monte Carlo, experiment, and sG theory are all in close agreement. The peak heights, however, are too small as given by the Monte Carlo calculation, and too large as given by the sG theory, when compared to experiment.

## 8.7 Discussion

Three possible reasons why the Monte Carlo calculation underestimates $\Delta C$ peak heights have already been suggested in section 8.6. An inappropriate assignment of the percent anisotropy can probably be ruled out, based on the evidence of Figure 8.8. From this present study, no conclusion can be drawn about whether there are other nonmagnetic contributions to the specific heat measured experimentally; we could only speculate. It is likely, however, that the peak heights are underestimated as a result of the finite m Trotter approximation, as the trends with m in the data

suggest. It would be useful to know more specifically about the way the Trotter errors behave as a function of m and the other parameters to answer this question. Not being able to answer this question currently, nevertheless the Monte Carlo data appears to be consistent with the experimental results for $\Delta C$.

The sG theory seems to fit poorly to the experimental data, even when the soliton rest mass is renormalized. It overestimates the peaks in $\Delta C$ considerably compared to the experimental data. Quantum mechanics must limit the degree of excitation of all the degrees of freedom of the full quantum Hamiltonian much more than that given by the quantized sG theory. But probably we should re-iterate some previous comments, about the more obvious reasons for the failure of the sG theory. It seems to be of doubtful motivation to take the original quantum Hamiltonian, taking classical limit, than the sG limit, and then quantizing the classical sG theory, other than that it is analytically tractable. This seems to be an especially questionable approach in light of the fact that the sG theory does not even adequately describe the classical mechanics given by the full classical Hamiltonian.

We conclude that quantum effects are important in the spin-$\frac{1}{2}$ 1-D ferromagnet CHAB, especially since the classical sG ideal gas theory fits poorly, while the quantum Monte Carlo data is consistent with experiment without any adjustment of parameters. There is a possibility that this could be made more convincing by solving for the free energy using a transfer matrix method in place of the Monte Carlo algorithm, thereby eliminating the statistical error bars. Some effort has been made in this direction, but there is difficulty in accurately finding the largest eigenvalue of the transfer matrix, from which the free energy is obtained,

due to the large size of the transfer matrix. For instance, if one "transfers" in the spatial direction, on the 2-D effective lattice, then the transfer matrix will be $2^{2m} \times 2^{2m}$. On the other hand, transferring in the Trotter direction is not any better, especially since then the eigenvalues depend on m in a singular manner such that all the eigenvalues would be necessary to determine the free energy, when one takes the $m \to \infty$ limit. Generally, though, transferring in the spatial direction seems to be the most promising approach; at this point it is a matter of accurate numerical computation to make this transfer matrix approach successful.

In Chapter 9, quantum effects in a spin-1 model for $CsNiF_3$ are examined, in a manner similar to that done here. Presently there is a continuing controversy over the importance of quantum mechanics vs. classical mechanics for $CsNiF_3$, and it is hoped that this quantum Monte Carlo approach should be able to help decide this question.